Schizophrenia Bulletin
doi:10.1093/schbul/sbab030

Early NMDA Receptor Ablation in Interneurons Causes an Activity-Dependent E/I Imbalance in vivo in Prefrontal Cortex Pyramidal Neurons of a Mouse Model Useful for the Study of Schizophrenia

Diego E. Pafundo*, Carlos A. Pretell Annan, Nicolas M. Fulginiti, and Juan E. Belforte

Grupo de Neurociencia de Sistemas, Instituto de Fisiología y Biofísica "Bernardo Houssay" (IFIBIO-Houssay), Universidad de Buenos Aires y Consejo Nacional de Investigaciones Científicas y Técnicas (CONICET), Ciudad de Buenos Aires, 1121, Argentina

*To whom correspondence should be addressed; 2155 Paraguayst 7 floor, Ciudad de Buenos Aires, 1121 Argentina; tel: +54-11-5285-3309, fax: +54-11-5950-9500 ext 2142, e-mail: dpafundo@gmail.com

Altered Excitatory/Inhibitory (E/I) balance of cortical synaptic inputs has been proposed as a central pathophysiological factor for psychiatric neurodevelopmental disorders, including schizophrenia (SZ). However, direct measurement of E/I synaptic balance have not been assessed in vivo for any validated SZ animal model. Using a mouse model useful for the study of SZ we show that a selective ablation of NMDA receptors (NMDAr) in cortical and hippocampal interneurons during early postnatal development results in an E/I imbalance in vivo, with synaptic inputs to pyramidal neurons shifted towards excitation in the adult mutant medial prefrontal cortex (mPFC). Remarkably, this imbalance depends on the cortical state, only emerging when theta and gamma oscillations are predominant in the network. Additional brain slice recordings and subsequent 3D morphological reconstruction showed that E/I imbalance emerges after adolescence concomitantly with significant dendritic retraction and dendritic spine re-localization in pyramidal neurons. Therefore, early postnatal ablation of NMDAr in cortical and hippocampal interneurons developmentally impacts on E/I imbalance in vivo in an activity-dependent manner.

Key words: prefrontal cortex/dendritic retraction/parvalbumin/electrophysiology/adolescence/gamma oscillations

Introduction

Effective transfer of information in the neocortex relies on a correct balance between excitatory (E) and inhibitory (I) circuits.[1–3] Functionally, the maintenance of an E/I synaptic balance imposes a tight, but dynamic, control of pyramidal neuron (PN) activity with a network of diverse GABAergic interneurons providing a fine-tuned, selective brake on cortical excitation. In particular, parvalbumin positive (PV) interneurons have been involved in E/I balance not only because of their conspicuous control of PN firing and timing[4–6] but also because their activity is associated with *"divisive"* rather than subtractive inhibition, allowing a proportional inhibitory response to dynamic excitation within the cortical circuit.[7] Thus, optimal inhibitory control by PV and other interneurons is central to maintain E/I balance and preserve multiple cortical processes ranging from simple sensory processing to high cognitive functions.[8] Considering that it is well accepted that PV interneurons are affected in schizophrenia (SZ),[9–14] it is not surprising that an altered E/I balance has been proposed as a central pathophysiological factor for SZ.[15–18] However, evidence published connecting SZ with a synaptic E/I imbalance at cellular level is mostly based on indirect approaches[19,20] or on direct electrophysiological assessment of E/I balance in brain slices (ex vivo) in SZ-related animal models.[21–23] Accordingly, drawing conclusions from these methods presents considerable limitations regarding the physiological status of the E/I balance, which requires further in vivo studies.

We have previously shown that NMDA receptor (NMDAr) ablation predominantly in cortical GABAergic interneurons, including PV positive ones, during an early postnatal period preceding adolescence results in SZ-related phenotypes after animals reach adulthood.[24] Moreover, triggering SZ-related phenotypes in adulthood depends on a developmental time window of susceptibility to NMDAr ablation.[25,26] Here, we provide evidence showing that this early NMDAr ablation results in unbalanced E/I inputs onto medial prefrontal cortex (mPFC) PNs in vivo during adulthood exclusively under a desynchronized cortical state presenting theta and gamma oscillations.

Methods

Full experimental procedures are described in the supplementary material.

Animals

Grin1 KO male and female mice lacking NMDAr in cortical and hippocampal GABAergic interneurons (mostly PV) were obtained by crossing Ppp1r2-Cre 4127$^{+/-}$ with Grin1^{tm2Stl} mice.[25] All animal protocols were approved by the University of Buenos Aires School of Medicine IACUC and government regulations (SENASA, Argentina). Preadolescent mice were studied between postnatal day 28 to 31 (hereafter juvenile), while 14 to 24 weeks-old mice constitute the adult group.

Brain Slice Electrophysiology

Electrophysiology was performed in mPFC coronal slices, recording mainly from prelimbic region, similarly as before.[27–29] Standard voltage clamp procedures were used to assess spontaneous and miniature excitatory and inhibitory postsynaptic currents in layer 2/3 PNs (supplementary material). Excitatory events were detected by voltage clamping PNs at −60 mV; inhibitory events, by measuring outward currents at 0mV. In our recording conditions, −60 mV and 0 mV represent the reversal potential for inhibitory and excitatory currents (supplementary figure S1). Spontaneous and miniature events were identified using Mini Analysis software (Synaptosoft) and validated by visual inspection. Intrinsic membrane and action potential properties were assessed in current clamp experiments.

In vivo Electrophysiology

Adult mice were anesthetized with urethane and mounted on a stereotaxic frame. Whole-cell voltage clamp recordings of mPFC PNs were performed mostly on the cingulate/prelimbic interphase region at 1.23 ± 0.04 mm (control) and 1.28 ± 0.04 mm (KO) of depth from brain surface on the right hemisphere, through a recording chamber. EEG was recorded over the contralateral mPFC (AP = 2 mm, ML = −0.5 mm).

Periods of recordings where the mPFC was in synchronized or desynchronized state were determined by the presence of strong delta oscillatory activity or the presence of theta/gamma oscillatory activities, respectively.[26,30] Spontaneous excitatory and inhibitory events were detected and measured from those sections as explained in the detailed materials and methods for slice experiments.

Histological Processing and Morphological Reconstruction of Neurobiotin-Filled Neurons

After whole-cell recordings, slices were quickly fixed and incubated with streptavidin-Cy3 (1:500 Invitrogen). Three-dimensional reconstructions of the dendritic arbor were performed and analyzed from fluorescence image stacks using the Neurolucida tracing system (MBF Bioscience). Dendritic spines were estimated from a single basal (3rd order) and a single apical (3rd order in the apical tuft) dendrite randomly selected for each PN (~100 µm of dendrite).

Immunohistochemistry

Floating coronal sections (30 µm) of perfusion-fixed mouse brains were stained with rabbit antibody to PV (PV27, Swant) and mouse to NeuN (MAB377, Millipore) followed by anti-rabbit Alexa 488 and anti-mouse Cy3 (1:500, ThermoFisher).

Quantification and Statistical Analysis

Results are expressed as mean ± SEM, and all bar plots are shown along individual data. Significance between group means was determined using paired or 2 sample *t*-tests or ANOVA, as indicated in each case. As indicated, when normality (estimated with Shapiro-Wilk or Kolmogorov-Smirnov tests) was rejected, natural logarithm transformation of data was used (in figures, data is shown without transformation). Significant *P* values are indicated in the Results and Figure Legends and all statistical values, number of cells, and animals used in each experiment are shown in supplementary table 1. No animals or neurons fulfilling our quality inclusion criteria were excluded from the analysis. Analyses were conducted in SPSS (IBM Analytics) and Statistica (StatSoft).

Results

In order to test the hypothesis that a selective ablation of NMDAr in cortical and hippocampal interneurons results in an Excitation/Inhibition (E/I) imbalance, we recorded the in vivo activity of mPFC PNs in voltage clamp mode under urethane anesthesia from adult control and mutant (KO) mice in which the NMDAr expression is abolished by ablation of Grin1 in a subset of cortico-hippocampal interneurons –mostly PV[25]– during early postnatal development (PD7-PD21). By simultaneously recording PN in whole-cell voltage clamp and the LFP in the contralateral mPFC (figure 1a), we were able to estimate the excitatory and inhibitory synaptic activity onto each recorded PN (figure 1b) during 2 different states of cortical activity: a slow wave state, with coordinated delta oscillatory activity reminiscent of natural Slow Wave Sleep; and periods of desynchronized state, with enhanced theta and gamma-related high-frequency components resembling wakefulness EEG (figure 1d–g). For instance, gamma power significantly increased over 2.5 times from synchronized to desynchronized state in both groups (control: 0.46×10^{-12} to 1.31×10^{-12}, KO: 0.61×10^{-12} to 3.80×10^{-12}, power spectral densities 40–50 Hz gamma band, median value of 7–8 mice, paired signed

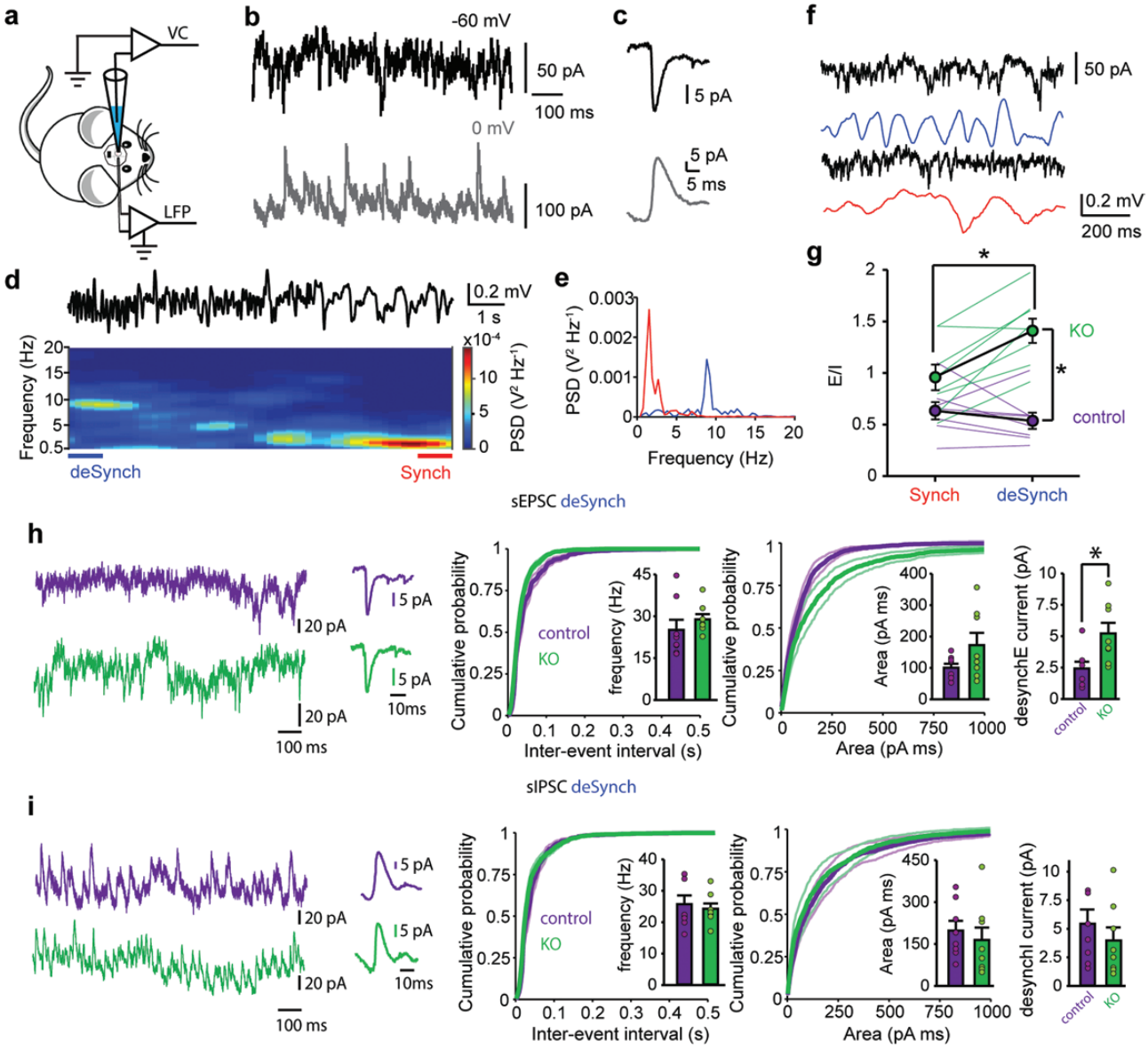

Fig. 1. Selective ablation of NMDA receptors on cortical and hippocampal interneurons results in Excitation/Inhibition imbalance of synaptic inputs to adult mPFC pyramidal neurons in vivo. (**a**) schematic reprsentation of recording conditions. (**b**) representative recordings of a pyramidal neuron (PN) voltage clamped at −60 mV (black, inward deflections represent EPSCs) and 0 mV (gray, outward deflections represent IPSCs). (**c**) average EPSC (black) and IPSC (gray) from (**b**). (**d**) example of a power spectral density (PSD) of the EEG with periods of synchronized (Synch) and desynchronized (deSynch) activity. Top: representative EEG recording, bottom: corresponding PSD analysis. The intervals of synchronized and desynchronized activity are color-coded and marked at the bottom. (**e**) PSD histogram for the periods highlighted in panel (**d**). (**f**) representative in vivo voltage clamp recordings of a PN, showing excitatory inputs in black for regions of deSynch (top) and Synch (bottom) periods. Contralateral mPFC EEG is plotted below each trace. (**g**), unbalanced Excitatory/Inhibitory inputs in PNs from KO mice during deSynch activity. Two-way repeated-measures ANOVA interaction $F_{1,14} = 8.14$, $P = .0013$. *$P < .05$ Sidak post hoc test. (**h–k**) analysis of spontaneous EPSCs (h) and IPSCs (i) in PNs from control and KO mice in vivo during deSynch activity. Left: voltage clamp recordings at −60 mV (excitatory inputs h) and 0 mV (inhibitory inputs i). Center left: average EPSC and IPSC from the examples shown on the left. Center: cumulative probability histograms for inter-event intervals for spontaneous EPSCs and IPSCs. The insets show averages. Center right: cumulative probability histograms for the inputs area. The insets show averages. Right: total current (mean area s^{-1}) for each input. *$P < .05$, t-test sEPSC $t_{14} = 2.79$, $P = .014$. In all cases, data are mean ± SEM, $n = 8$ neurons from 7 to 8 mice for each group.

$P = .008$ and $P = .016$). Only neurons where excitatory and inhibitory inputs could be recorded in both states for the same neuron were included in the analysis. We found that interneuron NMDAr ablation early on postnatal development results in a significant E/I imbalance in vivo, when compared with their control littermates, with synaptic inputs to PNs showing a shift towards excitation in adult KO mice (figure 1g, 8 control, 8 KO mice).

Notably, the altered E/I balance is only evident when cortical activity, resembles that of awake states characterized by desynchronized global activity (figure 1g, deSynch). In contrast, during synchronized state dominated by slow delta rhythm, the E/I inputs remained balanced (figure 1g Synch). The in vivo recorded synaptic inputs did not change their amplitude, rise or decay time in the KO mice in comparison to controls (supplementary figure S2), and whereas we were not able to detect significant changes in the frequency or in the integrated current of the inputs during synchronized state (supplementary figure S2), the PNs of KO mice received an increased excitatory drive during desynchronized global brain states compared with control (figure 1h). Given that the inhibitory drive remained within control levels (figure 1i), the E/I imbalance reported during cortical desynchronization was likely to result from an excess of excitatory drive to PNs in KO mice. Thus, these findings indicate that a state-dependent E/I imbalance emerges in mutants during periods of elevated information-processing demands and is not the sole consequence of the NMDAr ablation per se.

To dissect the underlying network mechanisms involved in the E/I imbalance, we next recorded layer 2/3 PNs of mPFC in brain slices from adult control and KO mice (figures 2a–c). All neurons recorded had common PN membrane and firing properties, with typical pyramidal shape and dendrite arborization (figures 2c–i). PNs from KO mice, however, displayed significantly higher input resistance (IR, 66%), slower membrane time constant (tau, 34%), and subsequently higher excitability (26% lower rheobase) than control mice with no differences in other membrane properties (supplementary figure S3). In order to estimate the E/I ratio of synaptic inputs arriving to PNs in the mPFC, we recorded excitatory (EPSCs) and inhibitory (IPSCs) currents in the same neuron by voltage clamping at −60 mV and 0 mV in the absence (spontaneous) and presence (miniatures) of TTX. We found that, while the frequency of miniature EPSCs (mEPSCs) was preserved in the KO mice compared to controls, the miniature IPSC (mIPSC) frequency was significantly reduced (41%, figures 2j and 2k). On the other hand, the magnitude of the inputs was not significantly different between KO and controls. In correspondence to the reduced mIPSC frequency, the neurons of the KO mice showed a significant shift in the E/I balance of the miniature currents towards excitation (figure 2l), thus suggesting that the main cause for the imbalance in the E/I ratio might be at the functional connectivity of the inhibitory synapses. Surprisingly, neither the frequencies, magnitude, nor E/I ratio of spontaneous inputs, (spontaneous EPSCs [sEPSCs] and IPSCs [sIPSCs]) were altered in mutant PNs (figures 2m–o). Figure 2 shows that inputs to PNs of KO mice display a shift towards excitation in the miniature currents that is not manifested when some degree of synaptic activity is preserved in the slice. Importantly, neither amplitude, rise time nor decay time of miniature and spontaneous currents were altered in KO mice (supplementary figure S4).

Considering that postmortem examinations of PNs of PFC from schizophrenic patients have shown a number of morphological alterations, we next asked if there was a structural correlate to the changes in excitatory and inhibitory inputs. We estimated the excitatory inputs by measuring the dendritic spine density in mPFC PNs of juvenile and adult control and KO mice. For inhibitory inputs, we focused on perisomatic inhibition by quantifying perisomatic PV puncta over the PNs. PNs of juvenile KO mice exhibited morphological features comparable to control ones (figure 3). As expected, a significant reduction in dendritic spine density occurred during adolescence in control mice. In contrast, dendritic spine pruning was absent in KO PNs, that retained spine densities similar to juveniles PNs (figures 3a and 3b). Interestingly, the total number of dendritic spines was similar between adult groups in both the basal and apical dendrites (figure 3b, bottom). Perisomatic PV putative inputs were not significantly altered in PNs of KO mice (figure 3c and supplementary figure S5).

Previously, we have reported that several behavioral[12,25,31] deficits found in adult KO mice emerge during adulthood. Accordingly, the membrane and action potential properties were unaltered in the juvenile KO PNs (supplementary figure S6) and neither were the excitatory and inhibitory input properties nor E/I balance affected in the KO mice at this age (supplementary figure S6). Thus, early ablation of NMDAr is not sufficient to affect E/I balance in juvenile KO mice, suggesting that alterations in PNs and circuit properties—including synaptic remodeling—observed in adulthood possibly emerge during adolescence.

We next analyzed the dendritic structure and arborization of the PNs recorded in mPFC slices from juvenile and adult mice (figure 4 and supplementary figure S7). We found a similar dendritic complexity and arborization in PNs from juvenile control and KO mice by Sholl analysis of intersections and distance per section (figure 4b), whereas this same analysis indicated a reduction in the complexity of basal and apical arbors of PNs from KO adults (figure 4h). Among juveniles, neither total length (figure 4d), apical (figure 4e) nor basal dendritic length (figure 4f) was modified in mutant mice. On the other hand, total, apical and basal dendrites from adult KO mice were shorter than controls (figure 4j–l). Importantly, the number of PNs principal basal dendrites was similar in controls and KO of adult (8 ± 1.01 vs 6.6 ± 0.54, $P = .238$) and juvenile (6.45 ± 0.51 vs 6.17 ± 0.44, $P = .673$) mice indicating a reduction of the length and complexity of each tree. The volume covered by each PN, however, was not altered in KO mice, indicating that they receive inputs arriving to similar volumes (supplementary figure S7). Further analysis of the

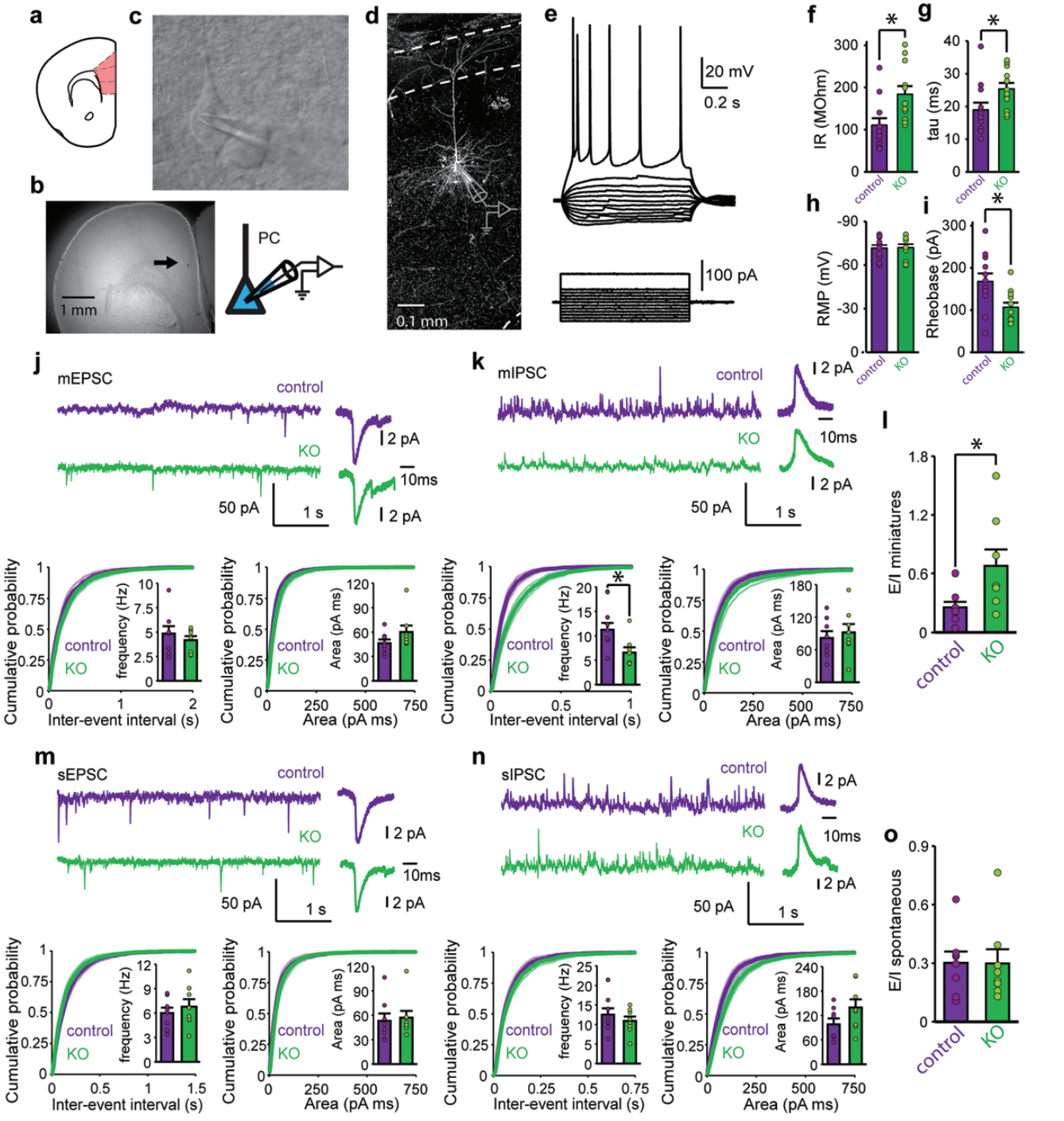

Fig. 2. MDAr ablation in interneurons increases mPFC pyramidal neurons excitability and alters inhibitory synaptic inputs. (**a**) schematic drawing of the mPFC areas in a mouse coronal slice. (**b**) arrow points a PN recorded in an mPFC slice. (**c**) infrared differential interference contrast image illustrating the recorded PN and the glass pipette. (**d**) z-maximal projection of a fluorescent image stack from the neurobiotin-filled PN shown in b and c. (**e**) membrane potential of the control PN shown in d in response to a series of subthreshold, and one suprathreshold, rectangular current injections. (**f–i**) intrinsic membrane properties of PNs recorded from control and KO mice. Input resistance (IR, **f**), membrane time constant (tau, **g**), resting membrane potential (RMP, **h**) and minimum current step that elicit an action potential (rheobase, **i**). n = 12 neurons from 6 mice per group. *$P < .05$, *t*-test, IR $P = .008$; tau $P = .035$; RMP $P = .845$; Rheobase $P = .011$. (**j–o**) Unbalanced E/I miniature synaptic inputs in PNs from KO mice. Analysis of miniature and spontaneous IPSCs (voltage clamped at 0mV, mIPSCs, and **k** sIPSCs, **n**) and EPSCs (voltage clamped at −60 mV, mEPSCs, **j** and sEPSCs, **m**). Top left: recordings from one control and one KO representative PN recorded in all 4 conditions. Top right: averaged detected inputs for top left traces. Bottom left: cumulative probability histograms for input inter-event intervals. Insets show averages. *$P < .05$ *t*-test: $t_{14} = 2.612$ mIPSC $P = .025$. Bottom right: cumulative probability histograms for inputs area. Insets show averages. E/I balance of miniature (**l**) and spontaneous inputs (**o**) were calculated as in vivo experiments. *$P < .05$, *t*-test: miniatures $t_{14} = 2.68$ $P = .042$. In all cases, $n = 8$ neurons from 4 mice for each group. Bar graphs depict data as mean ± SEM.

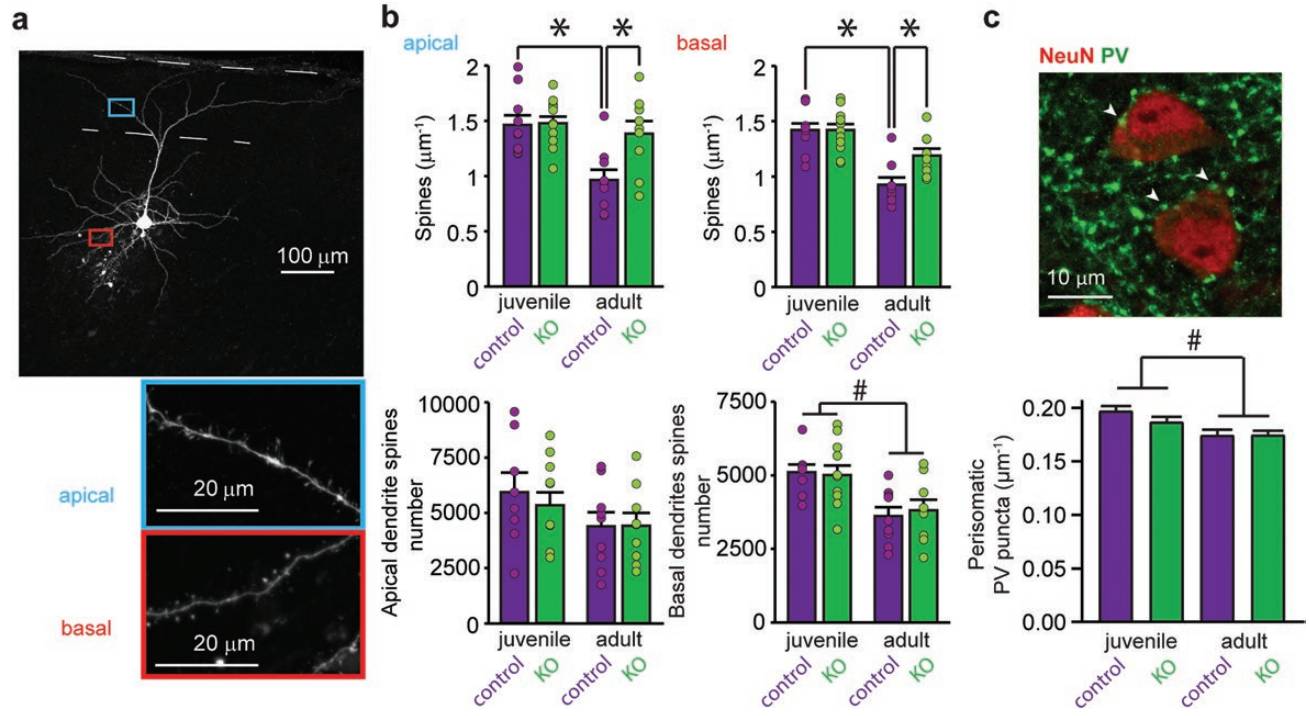

Fig. 3. Interneuron NMDAr hypofunction leads to dendritic spine re-localization in mPFC pyramidal neurons without changes in perisomatic inhibitory terminals density. (**a**) z-projection of a fluorescence stack of a representative neurobiotin-filled PN and zoomed-in images of sections of apical and basal dendrites. (**b**) top: spine density for apical and basal dendrites of mPFC PNs of juvenile and adult control and KO mice. Mean ± SEM $n = 10$ neurons from 4 to 6 mice per group. Two-way ANOVA interaction: apical: $F_{1,36} = 5.25$, $P = .028$; basal: $F_{1,36} = 4.70$, $P = .037$. *$P < .05$ Sidak post hoc test. Bottom: estimated total spines per neuron. Mean ± SEM, $n = 8$–10 neurons from 4 to 6 mice per group. Two-way ANOVAs Apical: no significant effects. Basal: age factor $F_{1,34} = 16.7$, $P = .001$, interaction $F_{1,34} = 0.26$, $P = .61$. # $P < .05$. (**c**) detail of a representative immunofluorescence image of a coronal mPFC slice, showing NeuN and PV labeling and mean number of perisomatic PV puncta of control and KO mice ($n = 260$–409 neurons from 9 to 14 mice). Two-way ANOVA: age factor $F_{1,1334} = 17.05$ $P = .001$, interaction $F_{1,1334} = 1.53$, $P = .21$. # $P < .05$.

total dendritic length from juvenile and adult control and KO PNs showed a significant interaction between age and genotype (figure 4m) arguing that the reduced dendritic lengths in adult KO PNs may result from dendritic retraction rather than from a reduced dendritic growth throughout development. Importantly, the ratio of apical vs basal dendrite length was not different between all 4 conditions (figures 4n and 4o), indicating a proportional pruning of dendrites in adult KO mice.

Discussion

Here we show an activity-dependent in vivo E/I imbalance of synaptic inputs to PNs of the prefrontal cortex in a previously validated mouse model useful for the study of SZ. We provide evidence that ablation of NMDAr in cortico-hippocampal interneurons, during early postnatal neurodevelopment, impacts on adult PNs at multiple levels resulting in increased excitability, dendritic retraction with spine re-localization, and altered excitatory and inhibitory inputs and balance. Importantly, these changes are not present before adolescence even though NMDAr ablation is already completed. Interestingly, the synaptic E/I imbalance detected at the network functional connectivity was masked in the PNs from KO mice by spontaneous activity in the slice, and also during in vivo synchronized activity under anesthesia. However, when inputs were measured in vivo during a desynchronized cortical state presenting theta and gamma oscillations, the KO mice prefrontal circuit displayed an activity-dependent E/I imbalance biased towards excitation that cannot be anticipated from previous *ex vivo* studies. Since physiologically relevant mPFC inputs from ventral tegmental area and ventral hippocampus complete their maturation during adolescence[32–34] and NMDAr ablation in cortical interneurons flattens induced –but not basal– mPFC dopaminergic release[24] and also impairs adult hippocampus-mPFC functional connectivity,[26] further studies will be required to assess the relative contribution of the local circuit and distal afferents to the altered E/I balance described. Also, ablation of NMDAr when animals reach adulthood may have a different impact on E/I balance or morphology than the ones reported here and must be addressed in further studies.

Whereas the functional connectivity deficits observed for miniature events in the slice lead to an E/I imbalance, we show that circuit activity can overcome the

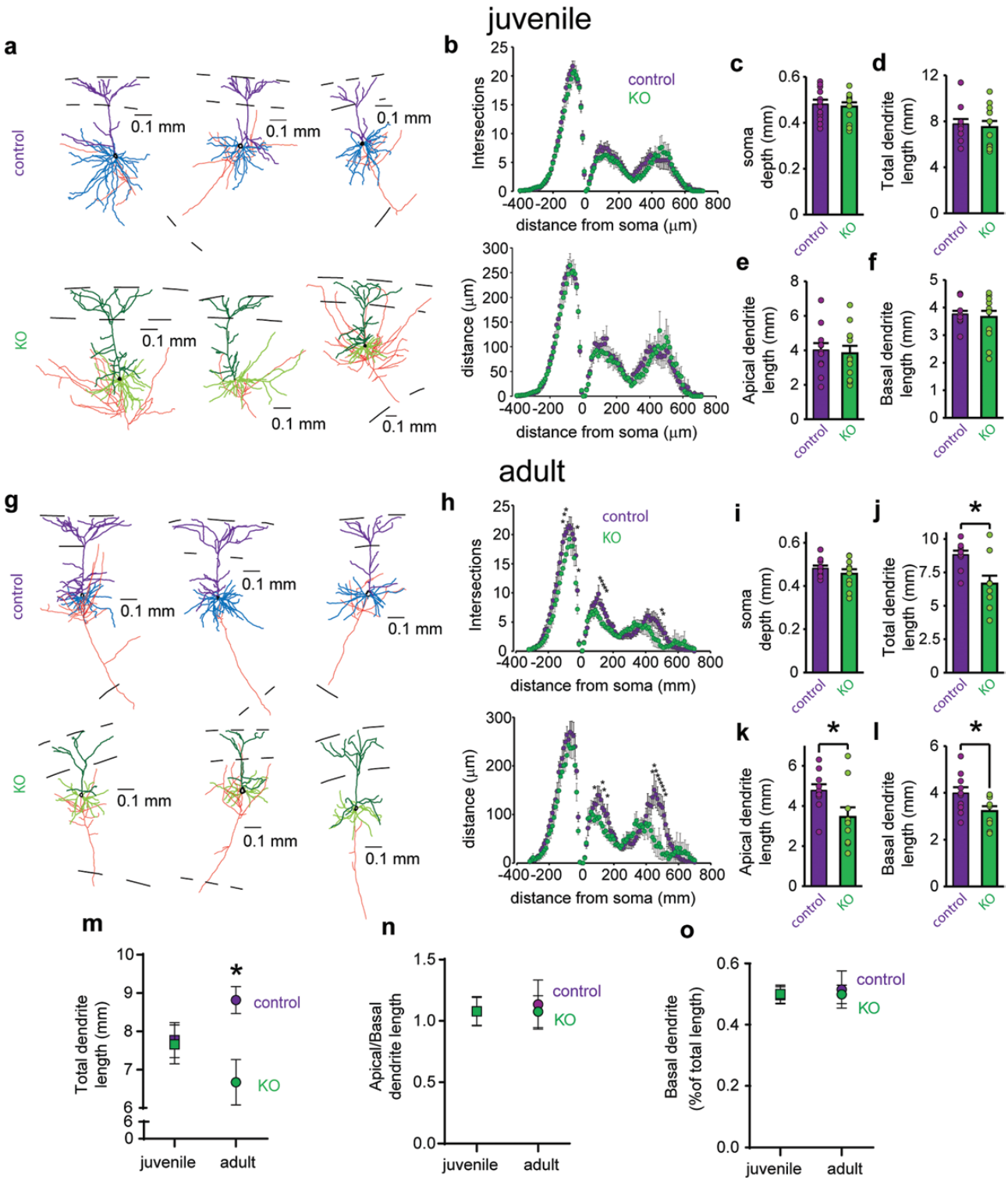

Fig. 4. Dendritic atrophy of mPFC pyramidal neurons emerges after adolescence in the interneuron NMDAr ablation mouse model. Analysis of morphological properties of PNs recorded and labeled in mPFC of juvenile (**a–f**) and adult (**g–l**) control and KO mice. (**a**) 3D Neurolucida reconstructions of representative PNs: soma shown in black; apical dendrites shown in dark thick lines; basal dendrites in lighter thick lines; and axon, in thin lines; controls and KOs as indicated for each row. The discontinuous lines depict from top to bottom: pia position, layer 1–2 border, and white matter (**b**) Sholl analysis of dendrite intersections (top) and distance (bottom) show no significant difference by 2-way repeated-measures ANOVAs. Sholl rings distance: 10 µm. Mean ± SEM, $n = 12$ for each group. (**c**) Location of recorded neurons. t-test: $P = .718$. Juvenile KO mice exhibit normal dendritic morphology without any significant difference by t-test in: total (**d,** $P = .87$), apical (**e,** $P = .77$), or basal (**f,** $P = .71$) dendritic lengths. (**g**) 3D digital rendering of adult PNs (control and KO mice, coding as in a). (**h**) NMDAr ablation reduces the complexity of dendritic arborization in adult KO mice (10 neurons per group

unbalanced inputs. In the KO mice, deficits in GABAergic interneuron activity and connectivity may lead to secondary prefrontal circuit alterations of network functions.[35] Thus, E/I imbalance emerges only under certain activity levels, specifically when unsynchronized cortical inputs arrive to the PNs, coinciding with an increase in theta/gamma oscillations. Accordingly, KO mice may display a crucial reduction in the dynamic range of cortical activity in which the network can balance E/I inputs. Indeed, the cognitive deficits observed in animal models of psychiatric disorders and SZ patients are related to high cognitive load and, concomitantly, high levels of asynchronous high-frequency oscillatory activity in the prefrontal network. Since network functions are highly dependent on the E/I balance,[8,36,37] one interesting speculation is that animals behave normally under low levels of circuit activity load in the mPFC, ie, during simple locomotion or basic visual processing.[25] But, when the mPFC is recruited for more cognitively demanding tasks, like working memory, the PNs of KO mice receive imbalanced E/I inputs biased towards excitation, predisposing the circuit to altered computations that could underlie the behavioral deficits observed. Similarly, it can be speculated that a reduced dynamic range of E/I balance could be present in human patients, since the cognitive capacity and functional deficits found in SZ appear to be related to the cognitive load during a variety of tasks, including item recognition[38] and working memory.[39]

Structurally, we found a marked dendritic retraction and spine reorganization in adult, but not juvenile KO mice. In particular, total spine number is conserved but their density is increased, thus synaptic integration in PN dendrites could be augmented and distal inputs could also have a stronger impact[40] and also a higher probability of producing dendritic action potentials due to a less complex tree,[41] resulting in an altered information filtering capacity. Putative perisomatic PV terminals over PNs were normal and frequency of miniature inhibitory inputs was reduced. This discrepancy can be attributed to changes in synaptic connectivity of other interneuron subtypes or in the functional properties of PV synapses. Importantly, a conserved number of PV interneurons and perisomatic PV puncta has also been reported in human SZ studies[42–44] suggesting a functional rather structural deficit in PV synapses.[10,45–47] However, since a subpopulation of Reelin positive interneurons may also be affected by our NMDAr ablation[25] we cannot rule out the possible contribution of other interneuron subtypes.

While PV-Cre transgenic lines may provide better cell-type specificity by exclusively targeting PV interneurons[48] recombination is not restricted to cortical areas and NMDAr ablation presumably occurs in all regions with strong PV expression, including thalamic reticular nucleus.[49] Moreover, when PV-Cre is used to ablate Grin1, recombination occurs late in postnatal development at around 8 weeks.[50] These regional and temporal differences may explain the apparent discrepancy in the behavioral profiles obtained after Ppp1r2-Cre vs PV-Cre mediated NMDAr ablation in relation to SZ-relevant phenotypes.[51]

In summary, early ablation of NMDAr in cortical and hippocampal interneurons triggers a series of compensatory changes in PNs that, although sufficient to sustain normal E/I balance in preadolescent mice, results in an activity-dependent alteration of E/I balance once the cortical circuit completes its maturation during adolescence.

Supplementary Material

Supplementary material is available at *Schizophrenia Bulletin* online.

Funding

This work was supported by Fondo para la Investigación Científica y Tecnológica (FONCYT) (PICT 2016-1807, 2018-0581, and 2016-0724), University of Buenos Aires (20020170100656BA), and Consejo Nacional de Investigaciones Científicas y Técnicas (CONICET), Argentina.

Acknowledgments

We thank Jésica Unger, Verónica Risso, Yamila Paez, Bárbara Giugovaz, Analía Lopez Diaz, and Graciela Ortega for technical assistance and Guillermo Gonzalez-Burgos and Kazu Nakazawa for critical reading of the manuscript. The authors have declared that there are no conflicts of interest in relation to the subject of this study.

from 6 to 7 mice). Sholl analysis of dendrite intersections (top) and distance (bottom). Two-way repeated-measures ANOVA showed for intersections a significant genotype × distance interaction for apical dendrites ($F_{69,1242} = 1.69$, $P = .009$) and significant main effect for genotype factor for basal dendrite ($F_{1,18} = 5.40$, $P = .032$) and for distance a significant interaction for apical dendrites ($F_{69,1242} = 3.01$, $P = .001$) without significant effects for basal dendrites. *$P < .05$, LSD post hoc test vs control. T-tests for **(i)**, soma depth ($P = .178$). **(j)** total dendritic length ($P = .008$). **(k)** length of apical dendrites ($P = .038$). **(l)** length of basal dendrites ($P = .035$). **(m–o)** comparison of morphological parameters across ages showed a global dendritic atrophy only when KO mice reach adulthood (**m**, 2-way ANOVA: genotype × age interaction $F_{1,38} = 4.18$, $P = .047$, *$P < .05$ Sidak post hoc test vs adult KO). Dendritic retraction in adult KO mice does not alter PNs apical/basal dendritic proportions. (**n** and **o**).

References

1. Desai NS, Cudmore RH, Nelson SB, Turrigiano GG. Critical periods for experience-dependent synaptic scaling in visual cortex. *Nat Neurosci.* 2002;5(8):783–789.
2. Turrigiano GG, Nelson SB. Homeostatic plasticity in the developing nervous system. *Nat Rev Neurosci.* 2004;5(2):97–107.
3. Liu Y, Zhang LI, Tao HW. Heterosynaptic scaling of developing GABAergic synapses: dependence on glutamatergic input and developmental stage. *J Neuroscience.* 2007;27(20):5301–5312.
4. Pouille F, Scanziani M. Enforcement of temporal fidelity in pyramidal cells by somatic feed-forward inhibition. *Science.* 2001;293(5532):1159–1163.
5. Wehr M, Zador AM. Balanced inhibition underlies tuning and sharpens spike timing in auditory cortex. *Nature.* 2003;426(6965):442–446.
6. Packer AM, Yuste R. Dense, unspecific connectivity of neocortical parvalbumin-positive interneurons: a canonical microcircuit for inhibition? *J Neuroscience.* 2011;31(37):13260–13271.
7. Ferguson BR, Gao WJ. PV Interneurons: critical regulators of E/I balance for prefrontal cortex-dependent behavior and psychiatric disorders. *Front Neural Circuits.* 2018;12:37.
8. Sohal VS, Rubenstein JLR. Excitation-inhibition balance as a framework for investigating mechanisms in neuropsychiatric disorders. *Mol Psychiatry.* 2019;24(9):1248–1257.
9. Lewis DA. Inhibitory neurons in human cortical circuits: substrate for cognitive dysfunction in schizophrenia. *Curr Opin Neurobiol.* 2014;26:22–26.
10. Lewis DA, Curley AA, Glausier JR, Volk DW. Cortical parvalbumin interneurons and cognitive dysfunction in schizophrenia. *Trends Neurosci.* 2012;35(1):57–67.
11. Dienel SJ, Lewis DA. Alterations in cortical interneurons and cognitive function in schizophrenia. *Neurobiol Dis.* 2019;131:104208.
12. Nakazawa K, Zsiros V, Jiang Z, et al. GABAergic interneuron origin of schizophrenia pathophysiology. *Neuropharmacology.* 2012;62(3):1574–1583.
13. McNally JM, McCarley RW, Brown RE. Impaired GABAergic neurotransmission in schizophrenia underlies impairments in cortical gamma band oscillations. *Curr Psychiatry Rep.* 2013;15(3):346.
14. Do KQ, Cuenod M, Hensch TK. Targeting oxidative stress and aberrant critical period plasticity in the developmental trajectory to schizophrenia. *Schizophr Bull.* 2015;41(4):835–846.
15. Lisman J. Excitation, inhibition, local oscillations, or large-scale loops: what causes the symptoms of schizophrenia? *Curr Opin Neurobiol.* 2012;22(3):537–544.
16. Gao R, Penzes P. Common mechanisms of excitatory and inhibitory imbalance in schizophrenia and autism spectrum disorders. *Curr Mol Med.* 2015;15(2):146–167.
17. O'Donnell P. Adolescent onset of cortical disinhibition in schizophrenia: insights from animal models. *Schizophr Bull.* 2011;37(3):484–492.
18. Jardri R, Hugdahl K, Hughes M, et al. Are hallucinations due to an imbalance between excitatory and inhibitory influences on the Brain? *Schizophr Bull.* 2016;42(5):1124–1134.
19. Dwir D, Giangreco B, Xin L, et al. MMP9/RAGE pathway overactivation mediates redox dysregulation and neuroinflammation, leading to inhibitory/excitatory imbalance: a reverse translation study in schizophrenia patients. *Mol Psychiatry*. 2020;25:2889–2904.
20. Molina JL, Voytek B, Thomas ML, et al. Memantine effects on electroencephalographic measures of putative excitatory/inhibitory balance in Schizophrenia. *Biol Psychiatry Cogn Neurosci Neuroimaging*. 2020;5(6):562–568.
21. Flores-Barrera E, Thomases DR, Tseng KY. MK-801 exposure during adolescence elicits enduring disruption of prefrontal E-I balance and its control of fear extinction behavior. *J Neuroscience.* 2020;40(25):4881–4887.
22. Del Pino I, Garcia-Frigola C, Dehorter N, et al. Erbb4 deletion from fast-spiking interneurons causes schizophrenia-like phenotypes. *Neuron.* 2013;79(6):1152–1168.
23. Marissal T, Salazar RF, Bertollini C, et al. Restoring wild-type-like CA1 network dynamics and behavior during adulthood in a mouse model of schizophrenia. *Nat Neurosci.* 2018;21(10):1412–1420.
24. Nakao K, Jeevakumar V, Jiang SZ, et al. Schizophrenia-like dopamine release abnormalities in a mouse model of NMDA receptor hypofunction. *Schizophr Bull.* 2019;45(1):138–147.
25. Belforte JE, Zsiros V, Sklar ER, et al. Postnatal NMDA receptor ablation in corticolimbic interneurons confers schizophrenia-like phenotypes. *Nat Neurosci.* 2010;13(1):76–83.
26. Alvarez RJ, Pafundo DE, Zold CL, Belforte JE. Interneuron NMDA receptor ablation induces hippocampus-prefrontal cortex functional hypoconnectivity after adolescence in a mouse model of schizophrenia. *J Neuroscience.* 2020;40(16):3304–3317.
27. Gonzalez-Burgos G, Miyamae T, Pafundo DE, et al. Functional maturation of GABA synapses during postnatal development of the monkey dorsolateral prefrontal cortex. *Cereb Cortex.* 2015;25(11):4076–4093.
28. Pafundo DE, Miyamae T, Lewis DA, Gonzalez-Burgos G. Presynaptic Effects of N-Methyl-D-Aspartate receptors enhance parvalbumin cell-mediated inhibition of pyramidal cells in mouse prefrontal cortex. *Biol Psychiatry.* 2018;84(6):460–470.
29. Pafundo DE, Miyamae T, Lewis DA, Gonzalez-Burgos G. Cholinergic modulation of neuronal excitability and recurrent excitation-inhibition in prefrontal cortex circuits: implications for gamma oscillations. *J Physiol.* 2013;591(19):4725–4748.
30. de Almeida J, Jourdan I, Murer MG, Belforte JE. Refinement of neuronal synchronization with gamma oscillations in the medial prefrontal cortex after adolescence. *PLoS One.* 2013;8(4):e62978.
31. Jiang Z, Rompala GR, Zhang S, Cowell RM, Nakazawa K. Social isolation exacerbates schizophrenia-like phenotypes via oxidative stress in cortical interneurons. *Biol Psychiatry.*.2013;73(10):1024–1034.
32. Tseng KY, O'Donnell P. Post-pubertal emergence of prefrontal cortical up states induced by D1-NMDA co-activation. *Cereb Cortex.* 2005;15(1):49–57.
33. Heng LJ, Markham JA, Hu XT, Tseng KY. Concurrent upregulation of postsynaptic L-type Ca(2+) channel function and protein kinase A signaling is required for the periadolescent facilitation of Ca(2+) plateau potentials and dopamine D1 receptor modulation in the prefrontal cortex. *Neuropharmacology.* 2011;60(6):953–962.
34. Gomes FV, Grace AA. Prefrontal cortex dysfunction increases susceptibility to Schizophrenia-like changes induced by adolescent stress exposure. *Schizophr Bull.* 2017;43(3):592–600.
35. Selten M, van Bokhoven H, Nadif Kasri N. Inhibitory control of the excitatory/inhibitory balance in psychiatric disorders. *F1000Research.* 2018;7:23.
36. Zhou S, Yu Y. Synaptic E-I balance underlies efficient neural coding. *Front Neurosci.* 2018;12:46.

37. Dehghani N, Peyrache A, Telenczuk B, et al. Dynamic balance of excitation and inhibition in human and monkey Neocortex. *Sci Rep.* 2016;6:23176.
38. Cairo TA, Woodward TS, Ngan ET. Decreased encoding efficiency in schizophrenia. *Biol Psychiatry.* 2006;59(8):740–746.
39. Honey GD, Bullmore ET, Sharma T. De-coupling of cognitive performance and cerebral functional response during working memory in schizophrenia. *Schizophr Res.* 2002;53(1–2):45–56.
40. Spruston N. Pyramidal neurons: dendritic structure and synaptic integration. *Nat Rev Neurosci.* 2008;9(3):206–221.
41. Major G, Larkum ME, Schiller J. Active properties of neocortical pyramidal neuron dendrites. *Annu Rev Neurosci.* 2013;36:1–24.
42. Hashimoto T, Volk DW, Eggan SM, et al. Gene expression deficits in a subclass of GABA neurons in the prefrontal cortex of subjects with schizophrenia. *J Neuroscience.* 2003;23(15):6315–6326.
43. Stan AD, Lewis DA. Altered cortical GABA neurotransmission in schizophrenia: insights into novel therapeutic strategies. *Curr Pharm Biotechnol.* 2012;13(8):1557–1562.
44. Guillozet-Bongaarts AL, Hyde TM, Dalley RA, et al. Altered gene expression in the dorsolateral prefrontal cortex of individuals with schizophrenia. *Mol Psychiatry.* 2014;19(4):478–485.
45. Fung SJ, Webster MJ, Sivagnanasundaram S, Duncan C, Elashoff M, Weickert CS. Expression of interneuron markers in the dorsolateral prefrontal cortex of the developing human and in schizophrenia. *Am J Psychiatry.* 2010;167(12):1479–1488.
46. Glausier JR, Lewis DA. Selective pyramidal cell reduction of GABA(A) receptor alpha1 subunit messenger RNA expression in schizophrenia. *Neuropsychopharmacology.* 2011;36(10):2103–2110.
47. Glausier JR, Lewis DA. GABA and schizophrenia: where we stand and where we need to go. *Schizophr Res.* 2017;181:2–3.
48. Hippenmeyer S, Vrieseling E, Sigrist M, et al. A developmental switch in the response of DRG neurons to ETS transcription factor signaling. *PLoS Biol.* 2005;3(5):e159.
49. Celio MR. Calbindin D-28k and parvalbumin in the rat nervous system. *Neuroscience.* 1990;35(2):375–475.
50. Carlen M, Meletis K, Siegle JH, et al. A critical role for NMDA receptors in parvalbumin interneurons for gamma rhythm induction and behavior. *Mol Psychiatry.* 2012;17(5):537–548.
51. Nakazawa K, Jeevakumar V, Nakao K. Spatial and temporal boundaries of NMDA receptor hypofunction leading to schizophrenia. *npj Schizophr.* 2017;3:7.